Vol. 6 • No. 1 • January 4 • 2018

www.advopticalmat.de

# ADVANCED OPTICAL MATERIALS

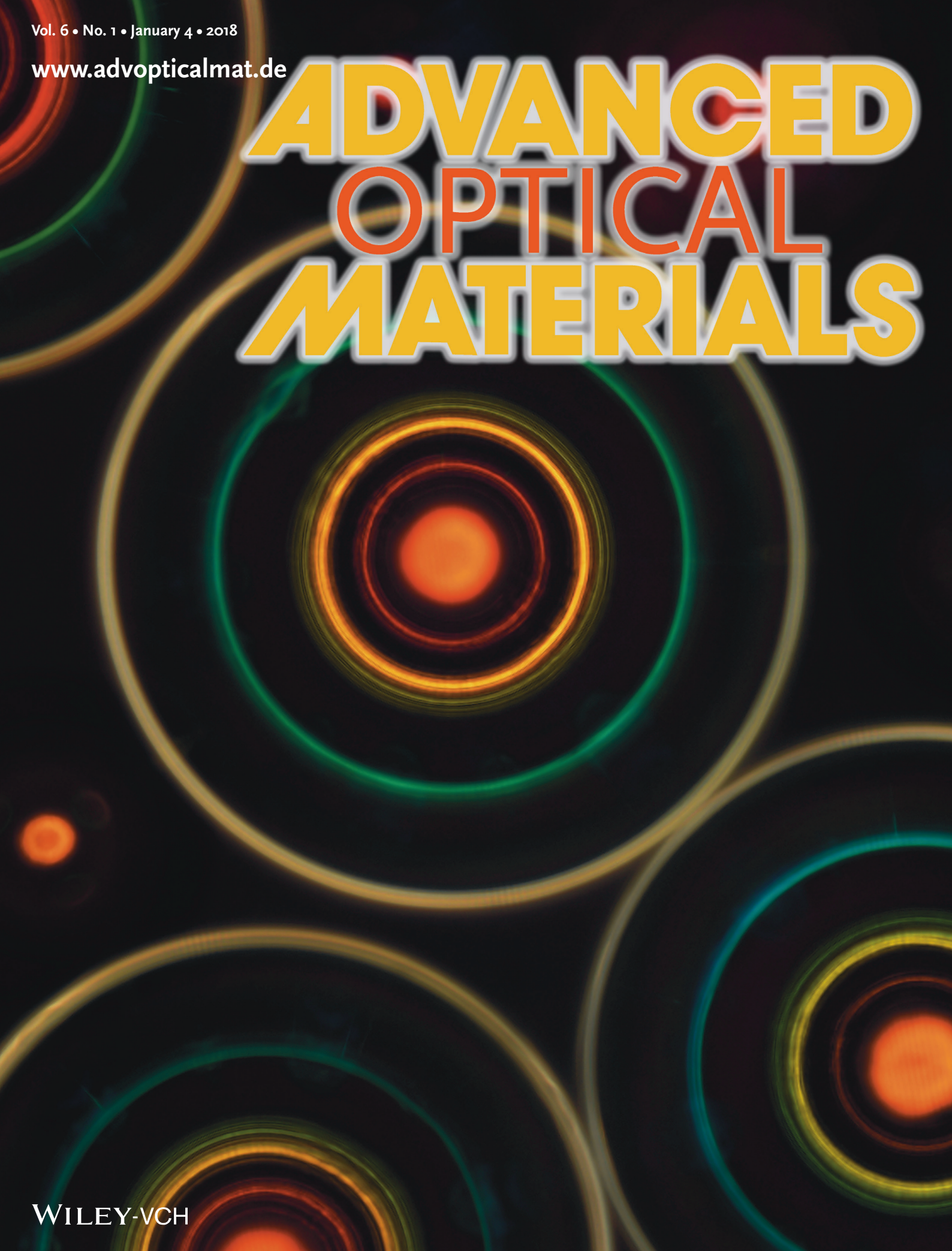

WILEY-VCH

ADVANCED OPTICAL MATERIALS
www.advopticalmat.de

# Through the Spherical Looking-Glass: Asymmetry Enables Multicolored Internal Reflection in Cholesteric Liquid Crystal Shells

*Yong Geng, Ju-Hyun Jang, Kyung-Gyu Noh, JungHyun Noh, Jan P. F. Lagerwall,* and Soo-Young Park**

**Spheres of cholesteric liquid crystal generate dynamic patterns due to selective reflection from a helical structure subject to continuously curved boundaries. So far the patterns are investigated exclusively as function of reflections at the sphere exterior. Here it is shown that the cholesteric shells in a microfluidics produced double emulsion enable also a sequence of internal reflections if the shells have sufficiently thin top and thick bottom. While such asymmetry is promoted by buoyancy when the internal droplet has lower density than the liquid crystal, the elasticity of the cholesteric helix prefers a symmetric shell geometry, acting against gravity. This subtle balance can hide the internal reflections for long time. Eventually, however, the asymmetry is established, revealing a new class of photonic patterns characterized by colored sharp concentric rings. With the complete knowledge of the diverse light-reflecting behavior of cholesteric liquid crystal shells, and utilizing the tunability of the structure period by, e.g., temperature, electric field, or exposure to various chemical species as well as polymer stabilization for making the shells long-term stable, they may be developed into remarkable new optical elements for photonics, sensing, or security pattern generation.**

## 1. Introduction

Cholesteric liquid crystals (ChLCs) are recognized as multitalented photonic band-gap materials[1] due to the combination of a spontaneous helix structure with tunable period (pitch, $p$), giving rise to optical Bragg reflection that responds dynamically to external influences,[2] and the processing ease that comes with a fluid state. Particularly attractive optical phenomena arise when ChLCs are curved into spheres[3,4] with radially aligned helix, for instance in droplets or shells (thin layer of ChLC surrounding an internal isotropic droplet). Among recently demonstrated or predicted manifestations of the potential of spherical ChLCs are omnidirectional tunable lasers[5] and chiral mirrors,[6] wavelength-selective photonic couplers/distributors,[7,8] photonic ink,[9] pH-, hydrogen peroxide and biosensors,[10–12] spontaneous nanoparticle segregation,[13] and unclonable patterns for secure authentication generated by arrays of ChLC shells.[14] So far, the optical properties were analyzed under the assumption that all light is reflected at the exterior of the ChLC and—with the exception of one paper suggesting a slightly ellipsoidal deformation[15]—that the droplets are perfect spheres, with full rotational symmetry. Is this assumption justified and does the neglect of possible deviations have consequences on the optical properties?

For shells, full rotational symmetry is not necessarily to be expected, since perfect density matching between the inner isotropic liquid and the surrounding ChLC phase is difficult to achieve, and because experiments have shown that at least a nonchiral nematic prefers asymmetric shells, as this allows minimization of the free energy cost related to topological defects.[16] While recent theoretical work[17] suggests that a short-pitch ChLC promotes symmetric shells with a close to central position of the inner droplet, this has until now not been experimentally corroborated. In this paper we show that ChLC shells can change over time from nearly symmetric to strongly asymmetric, via a close competition between symmetry-restoring elasticity of the cholesteric helix and symmetry disrupting buoyancy. We demonstrate that this variation in shell geometry has dramatic implications for the photonic behavior.

Symmetric shells and asymmetric shells with thick top (promoted by an inner phase denser than the ChLC) illuminated by white light from above behave as previously reported, exhibiting a pattern of colored spots generated by photonic

Dr. Y. Geng, J. H. Noh, Prof. J. P. F. Lagerwall
Physics and Materials Science Research Unit
University of Luxembourg
L-1511 Luxembourg, Grand Duchy of Luxembourg
E-mail: Jan.Lagerwall@lcsoftmatter.com
Dr. Y. Geng
Key Laboratory of Rubber-Plastics
Ministry of Education
Qingdao University of Science and Technology
Qingdao 266042, P. R. China
J.-H. Jang, K.-G. Noh, Prof. S.-Y. Park
Department of Polymer Science and Engineering
Polymeric Nanomaterials Laboratory
School of Applied Chemical Engineering
Kyungpook National University
80 Daehak-ro, Buk-gu, Daegu 41566, South Korea
E-mail: psy@knu.ac.kr
The ORCID identification number(s) for the author(s) of this article can be found under https://doi.org/10.1002/adom.201700923.

**DOI: 10.1002/adom.201700923**

 

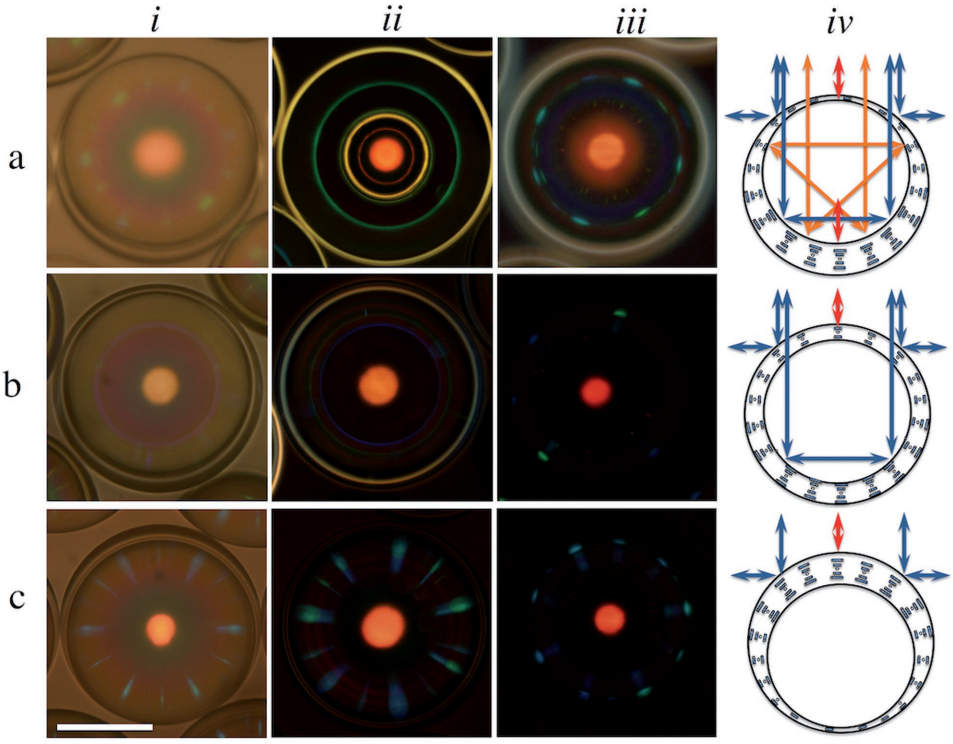


**Figure 1.** The optical signature of planar-aligned ChLC shells depends on their symmetry along the direction of light propagation. Row (a) shows reflection patterns of a shell that is very thin at the top and thick at the bottom (as defined by gravity). The asymmetry is seen in column (i), which shows the shell from the side. When viewed from the top (columns (ii) and (iii)) concentric internal reflection rings appear when the focus is close to the equator (ii), whereas crosscommunication spots[8] are visible with focus closer to the shell top (iii). The shell in row (b) is close to symmetric, with a shell top that is much thicker than in (a). It therefore shows fewer reflection rings in column (ii). The reduced number of spots in (b,iii) compared to (a,iii) is because the shell in (b) is more isolated than in (a). Row (c) shows a shell that is thicker on top than at the bottom. No internal reflection ring pattern can be seen, regardless of focus. Column (iv) shows schematic drawings of the reflection behavior in each shell type. Photos in columns (ii) and (iii) are obtained with crossed polarizers, while no polarizers were used for the photos in column (i). The scale bar is 100 µm.

crosscommunication between adjacent shells.[8,14] In contrast, if the ChLC shells are asymmetric with thin top (promoted by a less dense inner phase) an additional pattern of concentric colored rings arises, cf. **Figure 1**a, thanks to a sequence of selective reflection events taking place within the shell interior. This novel consequence of ChLC shell selective reflection, made possible when the shell top is too thin to completely divert the incoming light, is overlaid on the normal crosscommunication pattern, still visible at slightly different focus. We use a nested capillary microfluidic setup[18] to produce shells of different asymmetries, varying the compositions of the inner isotropic phase as well as of the ChLC (see the Supporting Information for details), and we investigate them by polarizing microscopy along and perpendicular to the direction of gravity. This way we can provide a complete picture of the complex optics made possible by ChLC shells and how the observed patterns sensitively reflect deviations from full rotational symmetry.

## 2. Results and Discussion

### 2.1. Shell Geometry and the Consequences of Shell Asymmetry for the ChLC Director Field

Depending on the composition of the ChLC mixture and of the inner phase, density mismatch and the resulting buoyancy force typically drive the inner droplet up or down, promoting shell asymmetry. The two ChLCs utilized in this work (see the Supporting Information) both have densities greater than water, thus an aqueous solution of polyvinylalcohol (PVA; added to stabilize the shell from collapse) as inner phase will tend to rise upward, giving the shell a thin top and thick bottom. An aqueous solution with 50% glycerol, used in our previous study,[14] is distinctly denser, promoting thin bottom and thick top.

In order to investigate the shell asymmetry, we fix a capillary filled with ChLC shells inside a hot stage mounted on the microscope, and the entire setup is tilted 90° while monitoring the texture with a camera attached to the microscope, cf. Figure S1 in the Supporting Information and resulting textures in Figure 1. The shell in the bottom row (c) in Figure 1 has a dense inner phase with 50% glycerol, sinking the inner droplet to the bottom. The shells in the two top rows (a and b) both have the same ChLC as in (c) and an inner phase that contains no glycerol. Interestingly, although this inner phase is less dense than the ChLC, only the shell in row (a) shows the expected asymmetry, with much thinner top than bottom. In contrast, the shell in row (b) is close to symmetric. The asymmetric shells of type (a) develop from the (b) type over the course of a few weeks. In the freshly prepared shell (b) the cholesteric structure is thus indeed acting against the effect of

buoyancy, promoting a positioning of the central droplet close to, but not quite at, the center of the shell, as expected from theory for a short-pitch ChLC.[17]

To confirm that the reduced asymmetry in (b) is due to the cholesteric phase, we heat the shell from room temperature to the isotropic state (transition at ≈60°C) in the tilted microscope, while continuously monitoring the shell shape, see Figure S2 and Movie S1 in the Supporting Information. The inner droplet remains close to the center throughout the cholesteric temperature range, but as soon as the isotropic state is reached the inner droplet rises, leaving a strongly asymmetric shell with very thin top after some 2 min. Cooling back to the cholesteric phase the asymmetric shape is now retained, showing that this shape represents the global energy minimum. This conclusion is further corroborated by long-term experiments showing that all shells without glycerol in the core were strongly asymmetric with thin top about two weeks after production.

It thus appears that the symmetric shell constitutes a local energy minimum when our ChLC surrounds the less dense aqueous internal phase. This local minimum is kinetically stabilized over a time scale of many days, with the consequence that the optical effects of shell asymmetry (discussed below) are hidden during experiments carried out soon after shell production. The question arises, what made the shell nearly symmetric in the first place, if this is only a local energy minimum. To understand this we investigate the high-speed video footage from the shell production, carried out with the ChLC heated to its isotropic phase temperature range, see Movie S2 in the Supporting Information. The slight deviations from symmetric geometry of the nested capillary channel leads to the shells being produced with liquid crystal predominantly close to one side, inducing a rapid rotation as soon as the shell is released from the production stream. The temperature is rapidly reduced as the shells are collected in a room temperature continuous phase, hence the ChLC mixture transitions into the cholesteric phase, with a consequent rapid increase in viscosity. In the process the ChLC material seems to be more evenly distributed around the shell, explaining the origin of the nearly symmetric shells soon after production.

Eventually buyoancy renders the shell asymmetric, however, and this geometry has interesting consequences for the director field on the in- and/or outside of the shell. Since the aqueous phases promote planar anchoring[20] (director in the interface plane[3]) the helix orients radially. As $p$ is constant throughout the shell, fewer helix turns fit in the thin part than in the thick part. Either or both of the interfaces with the surrounding isotropic phases will then constitute oblique cuts through the cholesteric structure, with a characteristic texture with a sequence of arches, see **Figure 2**. This texture is known as the "Bouligand cut" after Yves Bouligand, who first elucidated the phenomenon.[21] Bouligand cut textures have been analyzed and studied experimentally in many types of cholesteric liquid crystal, but most often for flat cuts. The asymmetric shells constitute an interesting example of spherical oblique cuts through a cholesteric with continuously varying helix orientation, where the characteristic arch texture is modulated by the nonconcentric spherical boundaries in combination with the radial helix.

Figure 2 shows an important consequence of the asymmetric position of the inner droplet: an energy penalty arises, either in terms of surface anchoring (deviation from the preferred planar alignment) or in terms of elastic deformation of the helix. The helix in the figure is drawn as would be promoted by the outer boundary, where the planar anchoring of the surrounding aqueous phase directs it radially inward. At the inner boundary, however, because the inner droplet is not at the shell center, the planar anchoring condition is violated. The alternative scenario, with planar anchoring respected on both interfaces, mediated via a bend in the helix from outer to inner boundary, may be more realistic. Either case raises the free energy compared to a central position of the inner droplet, providing a tangible illustration of why a short pitch ChLC promotes symmetric shells.

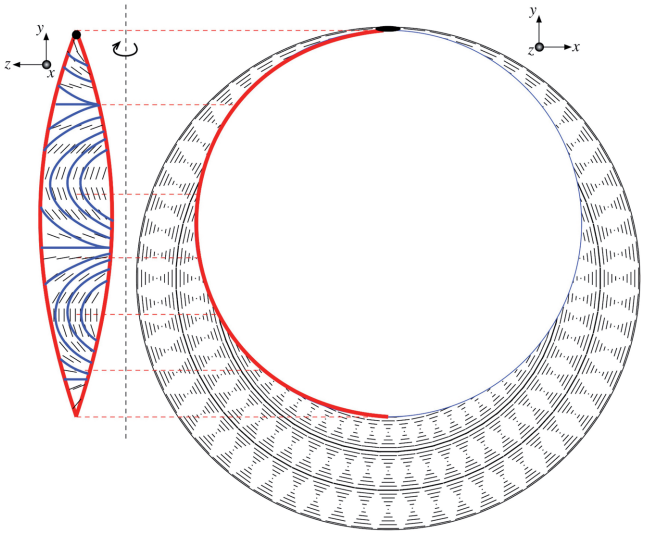


**Figure 2.** Schematic drawing of cross-section through an asymmetric ChLC shell with thin top. For simplicity, the helix is drawn with a pitch much longer than in the shells studied in this paper and its geometry is as promoted by the anchoring from the outside, thereby violating the planar anchoring on the inside. In reality the helix may bend to accommodate the planar anchoring at both boundaries. To the left a representative slice of the shell inside is drawn (as a projection onto the plane perpendicular to the paper, see the two coordinate systems for guidance) to illustrate the Bouligand cut director field that results from the nonconstant shell thickness. While multiple configurations of topological defects in the director field are possible, we have here chosen the case of a single $s = +2$ defect at the top[17,19] (indicated with a black dot).

While the director field cannot be free of topological defects in these planar-aligned shells, as dictated by topology and as demonstrated experimentally using long pitch cholesterics in planar alignment,[22] such defects have no impact on the reflection optical properties of these short pitch shells due to small sizes. In our study, the optics is governed by selective reflection from the cholesteric helix rather than by birefringence. Since the helix orientation is radial, there are no defects in the helix orientation field within the shell.

### 2.2. Rings from Internal Selective Reflection

Figure 1a(ii) clearly shows how a sequence of colored rings can appear in shells with thin top. As we will explain in the following, they arise from multiple consecutive selective reflection

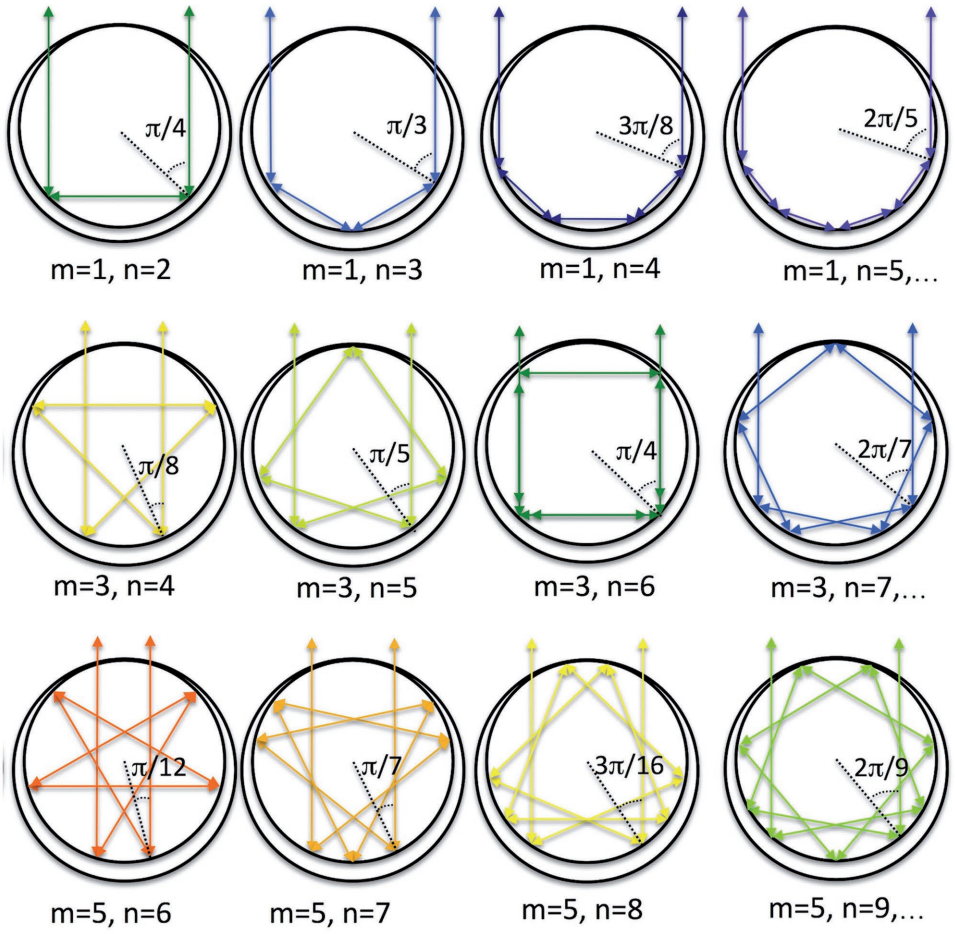


**Figure 3.** Schematic overview of 12 fundamental ring-generating internal reflection paths in ChLC shells with thin top, with varying apparent reflection angles $\theta_a$ (indicated at the first reflection). Inside the shell the light experiences $n$ reflections ($n$ = 1, 2, 3, ...) and at exit the ray direction has changed by $m\pi$ ($m$ = 1, 3, 5, ...). The paths are drawn in colors roughly corresponding to that of Bragg reflection, for a ChLC pitch giving deep red reflection along the helix ($\theta = 0°$), except for $m$ = 1; $n > 3$ which all yield reflection in the ultraviolet range for such a ChLC.

events at the shell inside (**Figure 3**). The shell's asymmetric geometry allows the microscope light to enter into the inner droplet and then to exit back up to the observer after the series of internal reflections. The selective reflection of ChLCs yields elliptically polarized light with the same handedness as the cholesteric helix, within a narrow band centered at the wavelength $\lambda = \overline{n}_{Ch}\, p \cos\theta$ (Bragg's law), where $\overline{n}_{Ch}$ is the average refractive index of the ChLC, $p$ is the helix pitch, and $\theta$ is the angle of incidence with respect to the ChLC helix ($\theta$ = 0° for incidence along the helix).

Several ring-generating internal reflection sequences are possible, Figure 3 schematically showing the 12 most fundamental ones, under the simplification that only the vertical exit direction is imaged. In reality the microscope objective will image reflection rings also with slightly nonvertical exit directions, due to its nonzero numerical aperture (NA; in our case NA = 0.3 and NA = 0.45, respectively, for the two objectives used). Below we will discuss the limitations of this simplification. The ring radius is equal to the lateral distance from the vertical symmetry axis to the last reflection point before the light exits through the shell top (see Figure S3, Supporting Information). For each path the apparent reflection angle $\theta_a$ is constant ($\theta_a$ is the reflection angle seen in the aqueous phase, defined with respect to the normal of the interface between water and ChLC). The number of times $n$ that the light is internally reflected increases from left to right, while the final reorientation angle of the light ray increases from top to bottom, as $m\pi$ radians, where $m$ must be an odd integer in order for the light to go back vertically to the observer. We index the different paths by their $m$ and $n$ values: ($m$, $n$). As elucidated in the Supporting Information, the requirement on $m$, together with the relation between $\theta_a$ and $n$ and the wavelength selection by Bragg's law, determine each ring's reduced radius (ring radius $r$ divided by shell radius $r_0$)

$$\sin\theta_a = \frac{r}{r_0} = \sin\frac{(n-m)\pi}{2n} \tag{1}$$

The apparent reflection angle $\theta_a$ is related to the incidence angle $\theta$ with respect to the cholesteric helix axis via Snell's law, introducing the refractive index of the aqueous phase $n_{aq} \approx 1.35$ and the average refractive index of the cholesteric, $\overline{n}_{Ch} \approx 1.52$

$$\frac{\sin\theta_a}{\sin\theta} = \frac{\overline{n}_{Ch}}{n_{aq}} \tag{2}$$

As explained in detail in the Supporting Information, we can then determine also each ring's wavelength

$$\lambda_r = \overline{n}_{Ch}\ p\cos\left(\arcsin\left(\frac{n_{aq}}{\overline{n}_{Ch}}\sin\frac{(n-m)\pi}{2n}\right)\right) \tag{3}$$

and also formulate a direct relation between ring wavelength and reduced radius

$$\lambda_r = \overline{n}_{Ch}\ p\cos\left(\arcsin\left(\frac{n_{aq}}{\overline{n}_{Ch}}\frac{r}{r_0}\right)\right) \tag{4}$$

The wavelength should thus be smaller the greater the radius. This conclusion is corroborated by our experiments, with the exception of the weak green ring seen outside the blue ring in Figure 1a,b(ii). This ring demonstrates that the nonzero NA of the microscope objective must be taken into account to explain all observed features. While the green-blue ring can be indexed (see below) as (5,9) for vertical entry/exit light path (see Figure S7, Supporting Information) we see in Figure 3 (drawn for slightly longer $\lambda_N = 670$ nm) that the (5,8) path includes two internal reflection events (no. 3 and no. 6 in the sequence) very close to the thinnest point of the shell prior to vertical exit. For a thin-topped shell the ChLC will allow some of the light to escape at this point and since the ray direction after the fifth reflection is rather close to vertical it can be imaged by the microscope objective due to its nonzero NA.[14] Since this path corresponds to a longer wavelength than the (5, 9) path we can now understand the origin of the (weak) outermost green ring.

Figure 3 also reveals that the visible reflections should be closer to the bottom, the smaller the ring radius. We should thus move from large-diameter short-wavelength rings to small-diameter long-wavelength rings as we focus from top to bottom within the shell. This is indeed what we see, as illustrated in **Figure 4** and Movie S3 in the Supporting Information, using a shell of a ChLC with red normal reflection ($\lambda_N = \overline{n}_{Ch}\ p \approx 650$ nm).

The ($m$, $n$) index of each ring is established by measuring the reduced radius of each ring and comparing with Equation (1) (tabulated values in the Supporting Information). This was done in Figure 4 and other examples are given in the Supporting Information. It may at first be surprising to see that even quite strong rings have their origin in internal reflection path with rather high $m$ and $n$ values. However, we are dealing with Bragg reflection: provided that a reflection takes place at a sufficiently thick point in the shell the reflection efficiency for the right wavelength and right polarization is very high. The first internal reflection selects exactly the wavelength band and polarization that is reflected by the ChLC in all following internal reflections. The ring intensity depends on how much light leaked out at reflections on the thin side prior to exit, and how much of the final upward-directed ray is allowed to leave the shell. In Figure 3 we have for clarity ended each internal reflection sequence after the first exit possibility, but a certain fraction of the light of course continues the internal reflection path.

A further experimental confirmation of our model is provided by illuminating only a fraction of a shell, see **Figure 5** and Movie S4 in the Supporting Information. We reduce the aperture and field diaphragms to their minimum openings (the latter is indicated by a dashed hexagon), and study a sample with an array of shells in reflection while translating it laterally. Initially (a) a shell with $\lambda_N \approx 580$ nm is at the center, being fully illuminated by the microscope. Significantly, as the shell is translated to the right the rings disappear *inside* the aperture area while they are still visible outside (c and d). Likewise, an adjacent shell, with $\lambda_N \approx 650$ nm, first becomes visible *outside* the illuminated area, while the illuminated part is fully invisible in (c). These observations prove the model in Figure 3, which is symmetric about the vertical shell center: in order to see a point in the shell, light must enter the shell at the *mirror point* on the other side. For a partially illuminated shell, we thus see the reflected light exiting outside the illuminated area, but in the illuminated area we see no reflection, since the entry point of that reflection path is not illuminated.

The helical structure of the cholesteric phase determines not only the wavelength of reflection but also the polarization: light reflected along the helix is circularly polarized with the same handedness as the helix. If it is obliquely reflected the handedness is retained but the polarization gains in ellipticity with increasing incidence angle $\theta$.[2] Because the ChLCs used in this work have right-handed helices we thus expect the internally reflected light, just like the communication spots, to be right-handed elliptically polarized, approaching circular polarization as the reflection ring diameter decreases (see Figure 3). We analyze the polarization dependence of the reflection patterns by varying the polarization of the illuminating light as well as the analyzer, see **Figure 6** and the Supporting Information. (A corresponding analysis in transmission can be found in ref. [23]).

When the shell is illuminated by right-handed circular-polarized light and the reflected light is analyzed by a right-handed circular analyzer (Figure 6a) the concentric rings are very clear and sharp. If instead left-handed circular polarizer and analyzer are used (b), all rings disappear except the bright white ring on the edge (to be discussed in

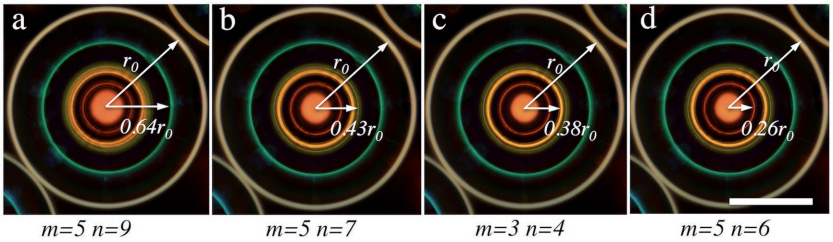


**Figure 4.** When changing the focal plane downward through the shell, the different rings come sequentially into focus, from large to small radius. The four most prominent rings (one blue and three green) are pictured in (a)–(d), their respective $m$, $n$ indices established by Equation (1) indicated below the figure. The scale bar is 100 µm.

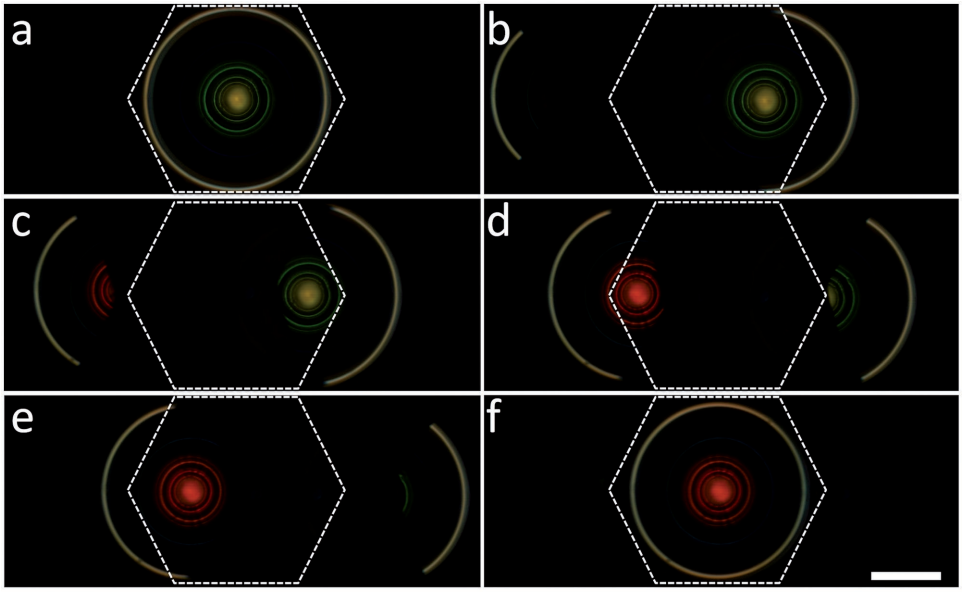


**Figure 5.** Reflection polarizing microscopy images (right-handed circular polarizer and analyzer) of ChLC shells moving from left to right across a small illuminated area (dashed hexagon). a) A shell with $\lambda_N \approx 580$ nm is fully illuminated. b–e) This shell is partially moved out of the illuminated area and a shell with $\lambda_N \approx 650$ nm is entering the illuminated area. f) The short-pitch shell no longer receives any light, leaving the long-pitch shell fully illuminated and visible. The scale bar is 100 µm.

the following subsection). As shown in the Supporting Information, the reverse configuration (left-handed polarizer and right-handed analyzer) gives similar results. If we examine the shell between crossed linear polarizers (Figure 6c) all colorful rings originating in the multiple internal Bragg reflection are present, with somewhat reduced intensity compared to the optimized situation in (a). The external bright ring differs from the inside rings through its intensity modulation, with minima at the extreme vertical and horizontal positions, an observation we will explain below. Without any polarizer (d), all rings appear more blurred due to an increased background of light reflected from the glass capillary and other interfaces.

As is clear from Figure 3 and Equations (1) and (3), our model predicts that the colors of the internal reflection rings depend on $p$, but the radius does not. The ring radius is set only by the geometry of the shell (ignoring the lensing effect from the shell top which also depends on $n_{aq}$ and $\overline{n}_{Ch}$). To confirm this, we produce shells using a ChLC mixture with temperature-tunable pitch, allowing us to study the effect of $p$ in one and the same shell. As shown in **Figure 7** the colors of the concentric rings indeed change as we change the temperature, and thus $p$, while the ring sizes are unchanged. Large rings become invisible for small $p$, as the ring color enters the UV range, while small rings leave the visible range into the IR regime when $p$ gets large. Any external parameter that influences the pitch of the ChLC should give rise to the same effect, thus monitoring of the ring color can be a powerful way of using ChLC shells in various sensing applications.

The reflectivity of the ChLC selective reflection depends on the average birefringence, thickness of the material, and the wavelength of the light.[24] In order for the light to at all enter into the inner droplet in order to trigger the internal reflection events that give rise to the rings, and then to be able to exit the shell again such that we can see the reflected light, the reflectivity at the shell top must not be too high. This explains why we only see rings clearly when the shell is very thin on top. The rings are entirely absent in asymmetric shells with thick top (Figure 1c), whereas the close to symmetric shell in (b) is a borderline case thanks to the slight reduction in thickness at the top compared to the bottom. Here we note that the inner rings are absent but the outer blue and green rings can be seen. At first this may seem surprising, since the shell top is thinner at the center than at the radii of the blue and green rings. To explain this, one must take the dependence on incidence angle of the reflectivity into account. The inner rings result from light entering close to the shell center, thus at small $\theta$, yielding higher reflectivity for the illuminating circular polarization than further out, where $\theta$ is greater and the reflectivity for circular polarization is lower.

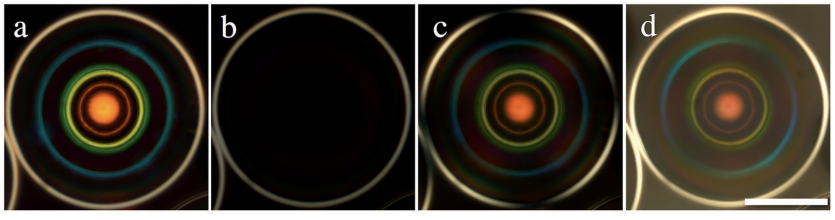


**Figure 6.** Reflection microscopy of a ChLC shell using different polarizer settings. In (a, b) the shell is illuminated by right and left-handed circular polarized light and viewed through a circular analyzer, right- and left-handed, respectively. In (c) the shell is between crossed linear polarizers and in (d) no polarizers are used. The scale bar is 100 µm.

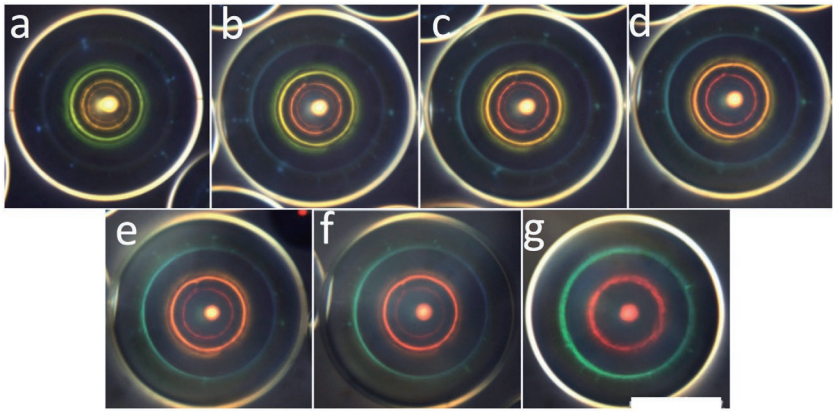


**Figure 7.** Reflection microscopy images (no polarizers) of a shell made of our ChLC2 mixture (details in the Supporting Information), with temperature dependent pitch $p$, during a heating experiment. The temperatures are a) 30, b) 35, c) 40, d) 45, e) 50, f) 55, and g) 60 °C. The ring radii are unaffected by $p$, but the colors change continuously, such that the outermost rings are difficult to identify at low temperature (small $p$) and the innermost rings at high temperature (large $p$). The scale bar is 100 µm.

### 2.3. Wavelength-Independent Total Internal Reflection (TIR) Leads to a Bright Perimeter of Thin-Topped Shells

We end this section by explaining the white perimeter that is seen in all thin- and medium thin-topped shells, but not in the thick-topped shells. This is not related to ChLC selective reflection, hence the lack of color and circular polarization. It is instead a result of TIR for light trapped *within* the ChLC layer itself, see **Figure 8**. While this light does not experience selective reflection, it does experience the birefringence of the ChLC, hence the dependence on linear polarization and the extinction of this ring at the extreme vertical and horizontal cross-sections of the perimeter, as seen in Figure 6c.

As light from the aqueous phase (refractive index $n_{aq} \approx 1.3$) reaches the shell interface, it is refracted against the interface normal, as on $\overline{n}_{Ch} \approx 1.5 > n_{aq}$. This couples the light into the shell, but it cannot easily leave it, since the next interface again borders an aqueous phase, with lower refractive index. As in an optical fiber the light is thus bounced between the interfaces, being guided along the shell. However, while an optical fiber has constant thickness, the asymmetric shells we are focusing on here get constantly thicker or thinner, depending on the side where the light enters. Combined with the spherical curvature of the interfaces this leads to a constantly changing reflection angle, and eventually the angle may be too small for TIR to take place, allowing the light to escape.

Figure 8a shows the case where light enters on the thick side of the shell. The light is initially guided within the shell, but this lasts only a short distance. The constantly decreasing shell thickness ensures that the reflection angle is soon reduced below the critical angle for TIR. No light is reflected back to the observer and the thick-topped shell appears with a dark rim in reflection (Figure 1c). In contrast, when light enters on the thin side of the shell (Figure 8b) there are several paths where TIR occurs all the way through the thick shell half, such that the light is reflected back to the origin. This explains why thin- and medium thin-topped shells appear with a bright white ring in reflection ((Figure 1a,b).

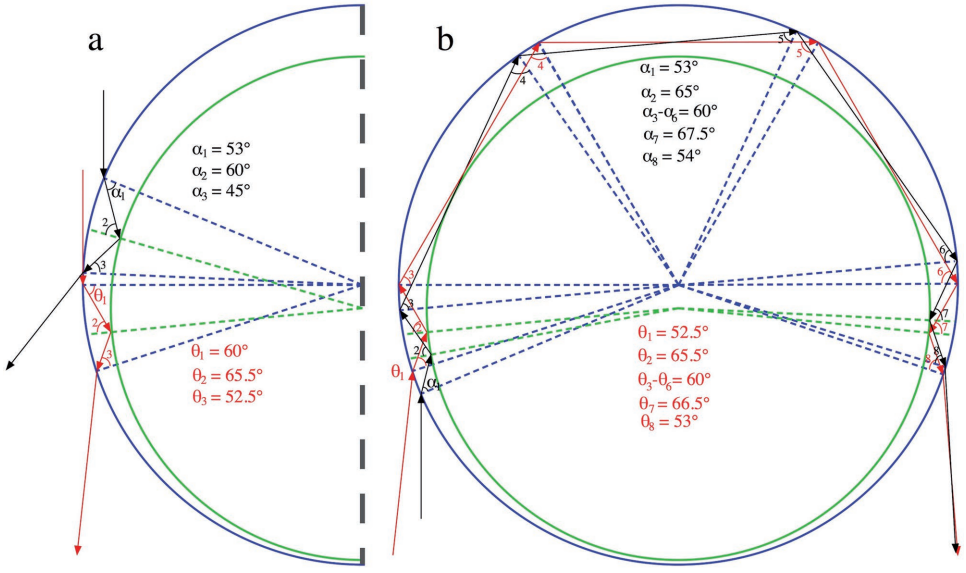


**Figure 8.** Schematic illustrations of the total internal reflection paths followed by light that enters into the actual ChLC shell, for entry on the thick side (a; only half the shell is shown) and on the thin side b). Two representative paths are indicated for each case, the consecutive reflection angles being $\alpha_x$ and $\theta_y$, respectively. For space reasons, only the indices $x$ and $y$ are indicated for $x$, $y > 1$.

## 3. Conclusions and Outlook

In summary, we have demonstrated how multiple internal Bragg reflection events can take place on the inside of cholesteric liquid crystal shells if the illuminated top of the shell is thin enough. We explain how these reflections give rise to a novel pattern with multiple sharp concentric rings, elliptically polarized with the same handedness as the cholesteric helix and with a color that is fundamentally determined by the helix pitch, being increasingly blueshifted with increasing ring radius. The cholesteric helix affects the behavior of the shells also through its elasticity, promoting a symmetric shell geometry against the effect of buoyancy for the common case of imperfect density matching between inner fluid and liquid crystal. This explains why the internal reflection pattern is frequently not visible soon after production. With an aqueous PVA solution forming the inside droplet it takes about two weeks before buoyancy wins, driving the less dense inner droplet to the top. This makes the shell sufficiently thin at the top for the internal reflection patterns to become visible.

The new mode of pattern generation significantly adds to the ability of ChLC shells to generate complex optical signatures that are difficult to clone and that can be as unique as a random combination of shell types allows.[14] Since the shells can be rendered long-term stable by polymerization of a small fraction of reactive mesogen added to the liquid crystal[14,25] this further raises the attractiveness of cholesteric liquid crystal shells in security applications. Moreover, the internal reflection may be very interesting to exploit in lasing, as we can use the tunability of the ChLC for varying the laser wavelength, yet the gain medium is the inner aqueous phase, which can be loaded with organic or inorganic dyes to an extent that is not possible in the ChLC itself. Finally, the complex optical signature combined with the sensitive response of cholesteric liquid crystals to external stimuli may make asymmetric shells very interesting in various sensing applications.[11,12] These are but a few of the possible application avenues of the versatile photonic material that cholesteric liquid crystal shells constitute.

## 4. Experimental Section

Two cholesteric liquid crystal mixtures were used in this work (details in the Supporting Information), one with strong temperature dependence of the pitch, the other relatively temperature independent. Both mixtures were based on an achiral nematic host phase to which a chiral dopant was added, its concentration setting the base pitch, and thereby the normal reflection wavelength $\lambda_N$ .

All shells were produced in nested glass capillary microfluidic devices, following the basic principle of Utada et al.[18] A detailed description is provided in the Supporting Information. The liquid crystal was heated to its isotropic phase and then flowed between aqueous solutions of PVA. Shell radius and thickness can be tuned by varying the flow rates of each fluid as well as the orifice sizes of the capillaries used.

The shells were filled into optically flat capillaries and then observed in reflection mode in a polarizing microscope. The capillary was kept in a hot stage for temperature control and the whole setup, including video camera mounted on the microscope, was tilted by 90° when observation perpendicular to gravity was desired (see the Supporting Information).

## Supporting Information

Supporting Information is available from the Wiley Online Library or from the author.

## Acknowledgements

Y.G. and J.-H.J. contributed equally to this work. Financial support from the National Research Foundation of Korea (NRF-2014R1A2A1A11050451), the European Research Council under the European Union's Seventh Framework Programme (FP/2007-2013)/European Research Council (ERC) Grant Agreement No. 648763 (consolidator project INTERACT), University of Luxembourg (project UNIQUE) is gratefully acknowledged. J.N. acknowledges support from the Fonds Nationale de la Recherche (FNR, Ph.D. grant ULISCO, code 6992111). The authors thank R. Sanctuary for the access to a refractometer for measuring refractive index.

## Conflict of Interest

The authors declare no conflict of interest.

## Keywords

cholesteric liquid crystals, double emulsions, selective reflection

Received: August 28, 2017
Revised: September 21, 2017
Published online: November 20, 2017

[1] a) A. Bobrovsky, K. Mochalov, V. Oleinikov, A. Sukhanova, A. Prudnikau, M. Artemyev, V. Shibaev, I. Nabiev, *Adv. Mater.* **2012**, *24*, 6216; b) D. J. Broer, C. M. W. Bastiaansen, M. G. Debije, A. P. H. J. Schenning, *Angew. Chem., Int. Ed.* **2012**, *51*, 7102; c) P. Cachelin, J. P. Green, T. Peijs, M. Heeney, C. W. M. Bastiaansen, *Adv. Opt. Mater.* **2016**, *4*, 592; d) M. Mitov, *Adv. Mater.* **2012**, *24*, 6260; e) J. Xiang, Y. Li, Q. Li, D. A. Paterson, J. Storey, C. T. Imrie, O. D. Lavrentovich, *Adv. Mater.* **2015**, *27*, 3014; f) Z. G. Zheng, Y. Li, H. K. Bisoyi, L. Wang, T. J. Bunning, Q. Li, *Nature* **2016**, *531*, 352; g) L. Wang, Q. Li, *Adv. Funct. Mater.* **2016**, *26*, 10; h) L. Zhang, L. Wang, U. S. Hiremath, H. K. Bisoyi, G. G. Nair, C. V. Yelamaggad, A. M. Urbas, T. J. Bunning, Q. Li, *Adv. Mater.* **2017**, *29*, 1700676; i) H. K. Bisoyi, Q. Li, *Chem. Rev.* **2016**, *116*, 15089.

[2] P.-G. de Gennes, J. Prost, *The Physics of Liquid Crystals*, Clarendon Press, Oxford, UK **1993**.

[3] M. Urbanski, C. G. Reyes, J. Noh, A. G. Sharma, V. S. R. Jampani, J. P. F. Lagerwall, *J. Phys.: Condens. Matter* **2017**, *29*, 133003.

[4] a) H. K. Bisoyi, Q. Li, *Acc. Chem. Res.* **2014**, *47*, 3184; b) Y. Iwai, Y. Uchida, N. Nishiyama, *Adv. Opt. Mater.* **2016**, *4*, 1961.

[5] a) Y.-L. Lin, L.-L. Gong, K.-J. Che, S.-S. Li, C.-X. Chu, Z.-P. Cai, C. J. Yang, L.-J. Chen, *Appl. Phys. Lett.* **2017**, *110*, 223301; b) L. J. Chen, L. L. Gong, Y. L. Lin, X. Y. Jin, H. Y. Li, S. S. Li, K. J. Che, Z. P. Cai, C. J. Yang, *Lab Chip* **2016**, *16*, 1206; c) L. Chen, Y. Li, J. Fan, H. K. Bisoyi, D. A. Weitz, Q. Li, *Adv. Opt. Mater.* **2014**, *2*, 845; d) Y. Uchida, Y. Takanishi, J. Yamamoto, *Adv. Mater.* **2013**, *25*, 3234; e) M. Humar, I. Musevic, *Opt. Express* **2010**, *18*, 26995.

[6] M. G. Donato, J. Hernandez, A. Mazzulla, C. Provenzano, R. Saija, R. Sayed, S. Vasi, A. Magazzù, P. Pagliusi, R. Bartolino, P. G. Gucciardi, O. M. Maragò, G. Cipparrone, *Nat. Commun.* **2014**, *5*, 3656.

[7] a) S. J. Asshoff, S. Sukas, T. Yamaguchi, C. A. Hommersom, S. Le Gac, N. Katsonis, *Sci. Rep.* **2015**, *5*, 14183; b) J. Fan, Y. Li, H. K. Bisoyi, R. S. Zola, D. K. Yang, T. J. Bunning, D. A. Weitz, Q. Li, *Angew. Chem., Int. Ed.* **2015**, *54*, 2160.
[8] J. Noh, H.-L. Liang, I. Drevensek-Olenik, J. P. F. Lagerwall, *J. Mater. Chem. C* **2014**, *2*, 806.
[9] a) S. S. Lee, S. K. Kim, J. C. Won, Y. H. Kim, S. H. Kim, *Angew. Chem., Int. Ed.* **2015**, *54*, 15266; b) S. S. Lee, B. Kim, S. K. Kim, J. C. Won, Y. H. Kim, S. H. Kim, *Adv. Mater.* **2015**, *27*, 627.
[10] Y. Iwai, H. Kaji, Y. Uchida, N. Nishiyama, *J. Mater. Chem. C* **2014**, *2*, 4904.
[11] H. G. Lee, S. Munir, S. Y. Park, *ACS Appl. Mater. Interfaces* **2016**, *8*, 26407.
[12] J.-H. Jang, S.-Y. Park, *Sens. Actuators, B* **2017**, *241*, 636.
[13] Y. Li, J. J.-Y. Suen, E. Prince, E. M. Larin, A. Klinkova, H. Thérien-Aubin, S. Zhu, B. Yang, A. S. Helmy, O. D. Lavrentovich, E. Kumacheva, *Nat. Commun.* **2016**, *7*, 12520.
[14] Y. Geng, J. Noh, I. Drevensek-Olenik, R. Rupp, G. Lenzini, J. P. F. Lagerwall, *Sci. Rep.* **2016**, *6*, 26840.
[15] J. Noh, I. Drevensek-Olenik, J. Yamamoto, J. P. F. Lagerwall, *Proc. SPIE* **2015**, *9384*, 93840T.
[16] A. Fernandez-Nieves, V. Vitelli, A. S. Utada, D. R. Link, M. Marquez, D. R. Nelson, D. A. Weitz, *Phys. Rev. Lett.* **2007**, *99*, 157801.
[17] Y. Zhou, A. Guo, R. Zhang, J. C. Armas-Perez, J. A. Martínez-González, M. Rahimi, M. Sadati, J. J. de Pablo, *Soft Matter* **2016**, *12*, 8983.
[18] A. Utada, E. Lorenceau, D. R. Link, P. D. Kaplan, H. A. Stone, D. A. Weitz, *Science* **2005**, *308*, 537.
[19] A. Darmon, O. Dauchot, T. Lopez-Leon, M. Benzaquen, *Phys. Rev. E* **2016**, *94*, 062701.
[20] J. Noh, K. Reguengo De Sousa, J. P. F. Lagerwall, *Soft Matter* **2016**, *12*, 367.
[21] a) Y. Bouligand, F. Livolant, *J. Phys.* **1984**, *45*, 1899; b) F. Livolant, M. Giraud, Y. Bouligand, *Biol. Cell* **1978**, *31*, 159.
[22] A. Darmon, M. Benzaquen, D. Seč, S. Čopar, O. Dauchot, T. Lopez-Leon, *Proc. Natl. Acad. Sci. USA* **2016**, *113*, 9469.
[23] Y. Geng, J. Noh, J. P. F. Lagerwall, *Proc. SPIE* **2016**, 9769, 97690U.
[24] a) W. D. S. John, W. J. Fritz, Z. J. Lu, D.-K. Yang, *Phys. Rev. E* **1995**, *51*, 1191; b) T. Scharf, *Polarized Light in Liquid Crystals and Polymers*, John Wiley & Sons, Inc., Hoboken, NJ **2007**.
[25] J. Noh, B. Henx, J. P. F. Lagerwall, *Adv. Mater.* **2016**, *28*, 10170.

 